Pergamon

Int. J. Heat Mass Transfer. Vol. 41, No. 15, pp. 2347–2360, 1998

Printed in Great Britain
0017–9310/98 $19.00+0.00

PII: S0017–9310(97)00361–X

Quantitative infrared-thermography for wall-shear stress measurement in laminar flow

R. MAYER, R. A. W. M. HENKES† and J. L. VAN INGEN

Delft University of Technology, Faculty of Aerospace Engineering, Kluyverweg 1, 2629 HS Delft, The Netherlands

(*Received* 21 *March* 1997 *and in final form* 20 *October* 1997)

Abstract—The hot film is a common technique to measure wall-shear stress in boundary-layer flows. A new technique to measure the wall-shear stress, referred to as quantitative infrared-thermography, has been developed. It replaces the internal heating and the temperature detection using the hot film with the external heating using a laser and the external temperature measurement using an infrared camera, respectively. First the laser creates a hot spot on a substrate of polycarbonate covered with a plastic foil; the conductivity of the chosen substrate is small and the emissivity is large, giving the required small, but clearly detectable spot. Then the laser is switched off and the temperature decay is monitored. The measured unsteady wall temperature is used as a boundary condition to numerically solve the heat transfer in the solid, which gives, through the total heat balance, the heat transfer from the solid to the fluid. A local similarity relation, which applies for small spots, is used to relate the wall-heat transfer to the wall-shear stress. The technique is demonstrated for the Blasius boundary layer in a wind-tunnel experiment, where an accuracy of about 10% has been achieved. © 1998 Elsevier Science Ltd. All rights reserved.

1. INTRODUCTION

When a solid body is placed in a fluid flow, normal and tangential stresses on the surface generate a certain lift and drag force. In wind-tunnel research the total forces on the object, such as models of airfoils, aircraft, cars and trains, can be measured with a force balance system. The sum of the pressure drag and skin-friction drag can also be found from the momentum-loss in the wake. For a detailed aerodynamic design of the object, however, it is often not sufficient to measure the total force, but the distribution of the stresses on the surface needs to be known. The normal stress (pressure) can easily be measured with a manometer connected to pressure orifices, but the measurement of tangential stress, i.e. the wall-shear stress, is more complicated.

Because of the importance of the wall-shear stress a variety of measurement techniques has been developed. The floating-element method directly measures the force on a small plate inserted flush into the surface of the object. The wall-shear stress can also be determined by measuring the velocity profile inside the boundary layer close to the wall with the help of a Pitot probe, hot-wire anemometry or laser-Doppler anemometry. Another measurement technique is the hot film. Since there is a relation between momentum and heat exchange, the wall-shear stress can be determined indirectly by measuring the heat transfer from a heated surface to the fluid (see e.g. Fage and Falkner [1]). Hot films comprise electrical heating and temperature measurement in the material of the surface of the film. The relation between the wall-heat transfer to the fluid (which is equivalent to the electrical power of the heater if the element is insulated from the solid) and the wall-shear stress is found by calibration (see e.g. Mathews and Poll [2]).

With certain simplifications an analytical similarity relation between the local wall-heat transfer and the local wall-shear stress can also be used. Based on this analytical relation a new type of hot film to measure the local wall-shear stress has been developed a few years ago at our laboratory in cooperation with the Faculty of Electrical Engineering of our university, which is called the integrated silicon flow sensor (Van Oudheusden [3]). This sensor consists of four electrical heating elements and four thermocouples, which are integrated in a sensor to measure the temperature differences in pairs. With the help of the measured temperature differences and the electrical power of the heating the two components of the wall-shear stress along the sensor surface can be determined.

Next to the classical hot-film technique infrared thermography (IR-thermography) can be applied to wall-shear stress measurements as well. IR-thermography has already been used qualitatively in aerodynamic research for a couple of years. Examples are the detection of transition from laminar to turbulent

† Author to whom correspondence should be addressed. Present address: Shell Research and Technology Centre, Amsterdam, P.O. Box 38000, 1030 BN Amsterdam, The Netherlands. Tel.: 31 20 630 3783. Fax: 31 20 630 2235. E-mail: Ruud.A.W.Henkes@opc.shell.com.

NOMENCLATURE

a	thermal diffusivity [m^2 s^{-1}]
c	specific heat capacity [J kg^{-1} K^{-1}]
c_f	wall-shear stress coefficient, $\tau_w/\frac{1}{2}\rho U_e^2$
h	solid thickness
k	thermal conductivity [W m^{-1} K^{-1}]
L	reference plate length [m]
q_f	wall-heat transfer at the fluid side [W m^{-2}]
q_{ir}	net irradiated laser power [W m^{-2}]
q_s	wall-heat transfer at the solid side [W m^{-2}]
T	temperature [K]
u, v	velocity components in x and y direction [m s^{-1}]
U_e	velocity at the boundary-layer edge [m s^{-1}]
x, y	coordinates along and normal to the plate [m].

Greek symbols

δ_T	thermal boundary-layer thickness [m]
δ_U	velocity boundary-layer thickness [m]
ΔT	temperature difference [K]
ζ	transformed y coordinate, $y[\tau_w/(\mu a(x-x_0)]^{1/3}$
Θ	dimensionless temperature $(T-T_e)/(T_w-T_e)$
Θ^*	dimensionless temperature $(T-T_e)/\Delta T$
μ	dynamic viscosity [kg m^{-1} s^{-1}]
ν	kinematic viscosity [m^2 s^{-1}]
ξ	dimensionless x-coordinate $(x-x_0)/L$
ρ	density [kg m^{-3}]
τ_w	wall-shear stress, $\mu(\partial u/\partial y)\|_w$ [N m^{-2}].

Subscripts

e	boundary-layer edge
f	fluid
s	solid
w	wall.

flow and separation bubbles in both windtunnel and flight tests. Transition and separation of the flow lead to a sudden change of the wall-shear stress and thus to a sudden variation of the wall-heat transfer. This leads to surface temperature differences on a heated object, which is monitored by an IR-camera. As long as the temperature resolution of the camera can detect these temperature variations, the precise value of the temperature itself is not of interest. This qualitative detection technique has been successfully applied to subsonic and transonic flows (Crowder [4]), as well as to hypersonic flows (Boerrigter and Charbonnier [5]). Qualitative IR-thermography with its rather simple experimental setup provides a fast and flexible measurement technique.

By combining IR-thermography with a numerical relation between the wall-shear stress and heat transfer to the fluid a new wall-shear stress measurement technique has been developed, which is presented in this paper. In contrast to qualitative IR-thermography, this new technique, which can be referred to as quantitative IR-thermography, is based on the accurate measurement of the surface temperature. As compared to the hot-film technique, the electrical heating of the hot film is replaced by externally irradiated energy from a laser and the internal surface temperature measurement is replaced by an external measurement performed by an IR-camera. In this new technique the laser heats up a hot spot until steady-state conditions are reached. After turning off the laser the camera measures the changing distribution of the surface temperature. From the measured temperature the heat transfer to the fluid and the wall-shear stress can be derived through a numerical procedure, as described in this paper. The measurement procedure is in fact a combination of measuring the decay of the surface temperature and numerically solving the equations for the velocity distribution near the surface and the temperature distributions in the flow and in the solid. The wall-shear stress is obtained by matching the computed and measured transient temperature distributions.

Compared to the hot film, quantitative IR-thermography offers three main advantages. Firstly, the measurement is non-intrusive, which means that the flow is not disturbed by the presence of a measurement probe. Secondly, the position of the measurement point can be easily changed by traversing the laser beam and the IR-camera. Thirdly, this technique can in principle be used on large scale objects, such as aircraft.

Section 2 introduces the relevant mathematical equations: boundary-layer equations for the velocity and the temperature in the boundary layer along the solid, and the Poisson equation for the temperature in the solid. If the heated spot remains small, the resulting temperature boundary layer is very thin compared to the velocity boundary layer and then a similarity solution for the temperature boundary layer can be used. The numerics to solve the equations are presented in Section 4. First some full numerical simulations of the fluid flow and the solid are made to optimise the chosen materials of the solid in relation to the required size of the hot spot. Then the simplified

analysis is presented. Sections 3 and 5 describe the experimental setup for the Blasius boundary layer along a flat plate in a windtunnel and the post-processing of the experimental data. Finally it is shown in Section 6 that the wall-shear stress for this pilot experiment on the plate could be measured with an accuracy of 10%. Suggestions for improving the accuracy are also given.

Although the procedure is demonstrated here for the Blasius boundary layer only, the same technique can be applied to boundary layers with a non-zero pressure gradient as well. Furthermore the technique is not only applicable to laminar boundary layers, but also to turbulent boundary layers. However, measuring the wall-shear stress in a turbulent boundary layer requires a smaller hot spot, to keep the thermal boundary layer within the viscous sublayer of the hydrodynamic turbulent boundary layer.

2. MATHEMATICAL FORMULATION

As mentioned in the introduction the relation between the local heat transfer to the fluid q_f and the local wall-shear stress τ_w has to be found. This investigation will be restricted to 2-D flow and 2-D heat transfer. For an incompressible laminar fluid flow the momentum and the heat transfer in the boundary layer can be described by the following boundary-layer equations

$$\frac{\partial u}{\partial x}+\frac{\partial v}{\partial y}=0 \tag{1}$$

$$u\frac{\partial u}{\partial x}+v\frac{\partial u}{\partial y}=-\frac{1}{\rho_f}\frac{\mathrm{d}p}{\mathrm{d}x}+\nu\frac{\partial^2 u}{\partial y^2} \tag{2}$$

$$\frac{\partial T}{\partial t}+u\frac{\partial T}{\partial x}+v\frac{\partial T}{\partial y}=a\frac{\partial^2 T}{\partial y^2}. \tag{3}$$

Here x and y are the coordinates along and normal to the wall, respectively; u and v are the corresponding velocity components; p is the pressure; and T is the temperature. The density, kinematic viscosity and thermal diffusivity of the fluid are denoted by ρ_f, ν and a, respectively, and can be assumed to be constant for the experiment described in the present paper. The diffusivity is defined as $a=(k_f/\rho_f c_{fl})$, where k_f is the conductivity and c_{fl} the specific heat capacity of the fluid. The velocity boundary layer [described by equation (2)] is steady and independent of the temperature. In contrast, the thermal boundary layer [described by equation (3)] depends on the velocity, and will be unsteady if the temperature of the surface depends on time.

Since the laser beam is very thin only a local small hot spot is generated. If the hot spot is sufficiently small the boundary-layer equations in the spot region can be further simplified. Using Taylor expansions in the spot region (which is assumed to start at x_0), the boundary-layer equations give

$$u(x,y)=\frac{\tau_w}{\mu}y+\frac{1}{2\mu}\frac{\mathrm{d}p}{\mathrm{d}x}y^2+\frac{1}{\mu}\frac{\mathrm{d}\tau_w}{\mathrm{d}x}(x-x_0)y + \text{3rd order terms} \tag{4}$$

$$v(x,y)=-\frac{1}{\mu}\frac{\mathrm{d}\tau_w}{\mathrm{d}x}y^2-\frac{1}{2\mu}\frac{\mathrm{d}^2\tau_w}{\mathrm{d}x^2}(x-x_0)y^2 - \frac{1}{6\mu}\frac{\mathrm{d}^2p}{\mathrm{d}x^2}y^3+\text{4th order terms}. \tag{5}$$

Hence we have to leading order:

$$u(x,y)=\frac{\tau_w}{\mu}y \quad \text{and} \quad v(x,y)=-\frac{1}{\mu}\frac{\mathrm{d}\tau_w}{\mathrm{d}x}y^2 \tag{6}$$

which only depends on the wall-shear stress, and is independent of the pressure gradient. As a consequence the same hot-spot technique, as described in this paper, applies to boundary layers with and without streamwise pressure gradients. Substituting the approximation (6) in the thermal boundary-layer equation (3) gives

$$\frac{\partial T}{\partial t}+\frac{\tau_w}{\mu}y\frac{\partial T}{\partial x}-\frac{1}{\mu}\frac{\mathrm{d}\tau_w}{\mathrm{d}x}y^2\frac{\partial T}{\partial y}=a\frac{\partial^2 T}{\partial y^2}. \tag{7}$$

In contrast to the velocity boundary layer, which starts to grow at the leading edge of the object, the thermal boundary layer starts at the position where the wall temperature first differs from the fluid temperature upstream of the hot spot. The velocity and the thermal boundary layers in the hot spot are sketched in Fig. 1(a). As long as the spot remains small the thickness of the thermal boundary layer δ_T is much smaller than the thickness of the velocity boundary layer δ_U. This implies that x derivatives of the velocity boundary layer (including $\mathrm{d}\tau_w/\mathrm{d}x$) are much smaller than x derivatives of the thermal boundary layer, which further simplifies (7) to

$$\frac{\partial T}{\partial t}+\frac{\tau_w}{\mu}y\frac{\partial T}{\partial x}=a\frac{\partial^2 T}{\partial y^2}. \tag{8}$$

This shows that for a sufficiently small spot, the thermal boundary layer approximately develops in a parallel flow with a linear velocity profile: the wall-shear stress is constant along the spot size. The maximum allowable spot size for equation (8) to hold will be determined in Section 4.2.

Equation (8) can easily be solved by a superposition of similarity solutions provided the unsteady term can be neglected. This is indeed allowable as the heat capacity of the air fluid layer ($=\rho_f c_{fl}\delta_T$ [J K^{-1} m^{-2}]) is much smaller than the heat capacity of the solid ($\rho_s c_s h$, with h being the thickness of the solid layer), particularly because $\rho_f \ll \rho_s$. This implies that the heat transported from the solid to the fluid is almost completely convected downstream in the fluid layer, whereas only a small portion is needed to locally heat up the fluid. The fluid almost immediately adjusts to

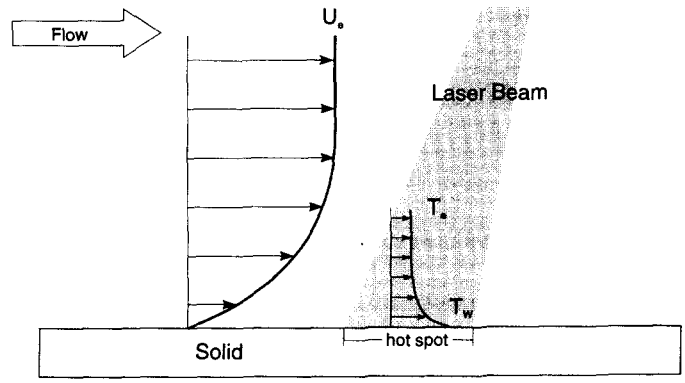

(a)

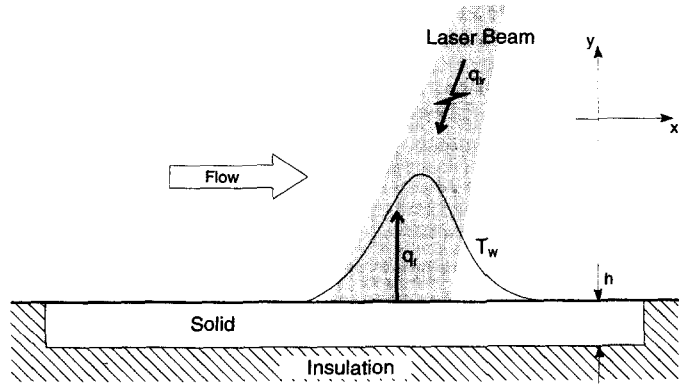

(b)

Fig. 1. Generation of a hot spot on a flat plate; (a) velocity and thermal boundary layer, (b) boundary conditions.

the temperature changes of the surface, and the thermal boundary layer can be treated as quasi-steady.

To find the similarity solution (see e.g. Lighthill [6]), we consider a sudden jump in the wall temperature from the ambient temperature T_e for $x < x_0$ to the constant temperature T_w for $x > x_0$. With $\zeta = y[\tau_w/(\mu a(x-x_0))]^{1/3}$ and $\Theta(\zeta) = (T-T_e)/(T_w-T_e)$, equation (8) (without $\partial T/\partial t$) can be transformed into

$$\Theta'' + \tfrac{1}{3}\zeta^2\Theta' = 0 \tag{9}$$

where a prime denotes differentiation with respect to ζ. Using the boundary conditions $\Theta(0) = 1$ and $\Theta(\infty) = 0$, the solution of this similarity equations reads

$$\Theta(\zeta) = 1 - C\int_0^{\xi} \exp\left(-\frac{1}{9}\zeta^3\right)\mathrm{d}\zeta \tag{10}$$

with $C = 0.5384$. Differentiation of the temperature gives the similarity solution for the wall-heat transfer q_f:

$$\frac{q_f L}{k_f(T_w - T_e)} = C\left(\frac{\tau_w L^2}{\mu a}\right)^{1/3}\xi^{-1/3} \tag{11}$$

where $\xi = (x-x_0)/L$ is a dimensionless coordinate in flow direction; $q_f = k(\partial T/\partial y)_w$ is the wall-heat transfer to the fluid; $\tau_w = \mu(\partial u/\partial y)_w$ is the wall-shear stress; L is an arbitrary reference length; and μ is the dynamic viscosity of the fluid. Since equation (8) is a linear differential equation in the temperature, the solution for an arbitrary surface temperature distribution can be written as a superposition of infinitesimal stepwise temperature variations at ξ^*. In this way equation (11) can be generalised to

$$\frac{q_f L}{k_f \Delta T} = C\left(\frac{\tau_w L^2}{\mu a}\right)^{1/3}\left[\Theta^*(0)\xi^{-1/3} + \int_0^{\xi}(\xi-\xi^*)^{-1/3}\frac{\mathrm{d}\Theta^*}{\mathrm{d}\xi^*}\mathrm{d}\xi^*\right] \tag{12}$$

where $\Theta^* = (T_w - T_e)/\Delta T$ is the dimensionless surface

temperature and ΔT is an arbitrary reference temperature difference; T_w is measured by the IR-camera. As the spot is smooth there is no jump in the wall temperature, which gives $\Theta^*(0) = 0$. For a given wall temperature, equation (12) relates the wall-heat transfer to the wall-shear stress.

For electrically heated hot spots, placed on a part of the surface which is thermally insulated from the solid, the heat transfer q_f to the fluid, integrated over the spot size, is given by the electrical power of the heater. However in the present IR-technique the magnitude of the irradiated laser energy and the heat loss into the solid are not known, which implies that an additional numerical procedure is needed to determine q_f from the measured wall temperature.

To do this, first the heat loss into the solid is determined from the unsteady 2-D heat-transfer equation for the solid (Poisson equation), which reads

$$\rho_s c_s \frac{\partial T}{\partial t} = k_s \left(\frac{\partial^2 T}{\partial x^2} + \frac{\partial^2 T}{\partial y^2} \right). \tag{13}$$

Here ρ_s, c_s and k_s are the density, specific heat capacity and thermal conductivity of the solid, respectively. Note that it is not assumed here that the surface is a thin plate for which the y dependence of the temperature has been eliminated and only x derivatives are retained. This will be discussed further in Section 4.1.

Boundary conditions are required to solve the Poisson equation (13). Except for the side facing the flow, where the wall-heat flux q_f is transferred, the three other sides are assumed to be perfectly insulated. The thermal boundary conditions for the solid are sketched in Fig. 1(b). The wall-heat transfer to the fluid q_f follows from

$$q_f = q_s - q_{ir} \tag{14}$$

with

$$q_f = \left(-k_f \frac{\partial T}{\partial y}\bigg|_w \right)_{\text{fluid}}, \quad q_s = \left(-k_s \frac{\partial T}{\partial y}\bigg|_w \right)_{\text{solid}},$$

and q_{ir} is the net irradiated power from the laser. If the laser is switched off ($q_{ir} = 0$), the heat fluxes at the surface fluid side (q_f) and solid side (q_s) are equal. Also if the laser is switched off, there is of course heat transfer by radiation from the hot spot. As the temperature of the spot remains relatively low (less than 20°C above ambient temperature), radiative heat transfer, though essential for the IR-camera, is negligible for the determination of q_f.

3. EXPERIMENTAL SETUP

To experimentally determine the wall-heat transfer, basically three different measurement methods can be applied:

- At time $t = 0$ the laser is switched on and starts to heat up the solid, which has an initial temperature equal to the ambient temperature. During the heating the IR-camera measures the increase of the surface temperature, from which q_f is derived.
- In the steady method the laser first heats up the solid, where after it continuously maintains the steady-state temperature in the hot spot, which is measured by the IR-camera.
- The laser heats up the solid until the temperature in the solid is steady, where after the laser is switched off and the IR-camera measures the temperature decay.

Performing the measurement while the laser is switched on (first and second method) would require the determination of the distribution of the irradiated power of the laser over the surface, which is difficult to do. Therefore, in this investigation the last method has been chosen, because it is independent of the irradiated power q_{ir}.

The performance and accuracy of the present measurement technique has been tested in a laminar flow along a flat plate without streamwise pressure gradient (so-called Blasius flow). The flat plate has been placed vertically in a closed wind tunnel with a cross section of 40×40 cm. The cross section of the measurement strip and the complete experimental setup are sketched in Fig. 2.

The plate consists of a 3 cm thick PVC base. The sharp nose is made of aluminium for manufacturing reasons. A series of holes in the plate measures the static pressure in streamwise direction. At the end of the plate a wooden flap is fixed to adjust the stagnation point and thus to avoid flow separation. Along the centerline of the plate a 1 mm polycarbonate strip is inserted flush into the PVC base. To increase the emissivity of the surface the polycarbonate has been covered with an 0.1 mm dull black plastic foil (Balageas [7]). As determined by the numerical simulation (see Section 4.2) this combination of polycarbonate and plastic foil seems to be a good compromise for the required spot size and decay time. Since the strip has to be inserted into the PVC base also a certain stiffness of the material is required. A 5 mm air sublayer has been milled underneath the measurement strip, which justifies the assumption of a perfect insulation as boundary condition in the numerical solution for the solid.

The required heating is provided by a nominally 5 W argon laser. As the heat transfer in the fluid and in the solid is limited to two dimensions, an oscillating mirror generates a laser sheet with a rather constant irradiated energy distribution spanwise to the flow. In this way a 2-D hot spot is generated and the energy is only transported in x- and y-direction, and not in spanwise direction. The mirror and the IR-camera are fixed on a traversing system to adjust the measurement position.

A common problem in IR-thermography in closed wind tunnel tests is the low transmittance of the wind tunnel walls [7]. To obtain a sufficiently strong signal

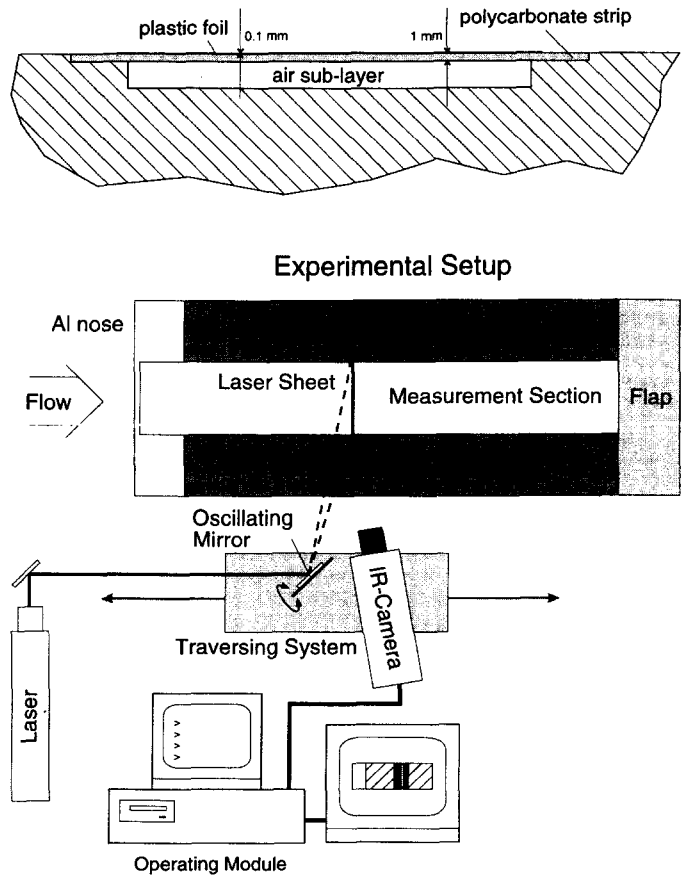

Fig. 2. Cross section of the measurement strip and the experimental setup (test plate is rotated by 90° around the horizontal axis).

a slit has been cut in the wall. This slit is covered with a thin transparent foil (0.05 mm), which reduces the irradiated power by not more than approximately 2%. As the foil is rather fragile, it can only be used for small static pressure differences between the inside and the outside of the wind tunnel.

4. NUMERICAL TREATMENT

4.1. *Full numerical simulation for the solid and the fluid*

To get more insight in the physics of the spot and to optimize the thickness and material choice of the solid, first a full numerical simulation was performed for a case that resembles a typical experimental situation. In this simulation a laser beam of 1 W with a diameter of 2 mm heats up the solid locally at $x = 0.2$ m. The irradiated power of the laser is taken constant along the beam diameter. The solid consists of a 1 mm polycarbonate strip and an 0.1 mm plastic foil. Along the surface a velocity boundary layer has developed from the leading edge with an outer-edge velocity of $U_e = 10\ \mathrm{m\ s^{-1}}$. When steady-state conditions are reached the laser is switched off at $t = t_0$, after which the temperature in the hot spot decays.

The numerical simulation of the solid and the fluid including the coupling procedure between the solid and the fluid, is straightforward and is certainly expected to have been used by others as well. First the velocities in the fluid are calculated from equation (2), which is discretized by a second-order finite-difference scheme. The boundary-layer equation is solved by a straightforward marching procedure for parabolic differential equations, which determines each new downstream flow station by solving tridiagonal matrices. The velocity boundary layer has to be computed only once because the flow is assumed to be steady and independent of the temperature. With the obtained velocities the temperature in the fluid can be calculated from the discretized equation (3), using a prescribed wall-temperature distribution. The coupling with the temperature in the fluid is established by the conditions that the temperature is continuous at the solid/fluid interface and that equation (14) is satisfied, which requires an iterative numerical procedure. The heat flux at the surface of the solid is collocated from the temperature gradient in the fluid perpendicular to the solid, as known from the previous iteration. If the laser is switched on the irradiated power along the surface is added. The resulting heat flux is prescribed as a Neumann boundary condition for the solid at the

side facing the flow. At the other boundaries of the solid homogeneous Neumann boundary conditions are prescribed. Herewith the temperature in the solid is computed. The unsteady Poisson equation in the solid (13) is discretized by a second-order implicit finite-difference scheme in space and time. At each iteration the resulting matrix equation is solved by using an LU-decomposition. This gives an update of the temperature at the surface, which is used as a boundary condition in the next iteration solving the thermal boundary-layer equation. The interaction process is stopped when changes in the wall-temperature have become less than a small convergence criterion.

Figures 3(a) and (b) present the resulting temperature distribution in y-direction and the x-dependent wall-heat transfer. When the laser has been switched off, the wall-heat transfer at the fluid side (denoted as a solid line in Fig. 3(b)) is equal to the wall-heat transfer at the solid side (dashed line). For $t = t_0$, just before turning off the laser, there is a difference between both wall-heat transfers, which is precisely equal to the prescribed local irradiated laser power.

In many applications of IR-thermography the temperature in the solid normal to the surface is assumed to be constant and the 2-D Poisson equation (13) is replaced by a 1-D approximation. Due to the low thermal conductivity and the unsteady heat transfer this approximation cannot be applied to the presented measurement technique. To clarify this, the 1-D and 2-D formulation are compared. In this comparison the solid consist of a single layer of polycarbonate with the thickness h. The 1-D heat-transfer equation can be obtained from equation (13) by integrating in y-direction under the assumption that the y-dependence of $\partial T/\partial t$ and $\partial^2 T/\partial x^2$ can be neglected. This gives

$$\rho_s c_s h \frac{\partial T}{\partial t} = k_s h \left(\frac{\partial^2 T}{\partial x^2}\right) + q_s. \tag{15}$$

Figure 3(c) shows the decay of the wall-heat transfer after switching off the laser as calculated for the 1-D and 2-D approaches for increasing thickness of polycarbonate (0.2, 0.5 and 1 mm). As expected, the difference in the wall-heat transfer becomes larger for increasing thickness. The difference is particularly large for short times after switching off the laser, when only the upper part of the solid close to the surface is cooled down. The comparison shows that even for 0.2 mm the 1-D approximation leads to small errors, which would be even larger if a two-layer solid with different thermal properties would have been simulated.

4.2. *Accuracy of the similarity relation between wall-heat transfer and wall-shear stress*

In the experimental method, the wall-shear stress is not known beforehand, but it precisely is the result of the measurement. The unknown wall-shear stress is coupled to the measured temperature and the computed heat transfer in the solid by using the similarity relation (12), which can only be applied as long as the spot remains small. The integral in equation (12) is evaluated by a second-order numerical scheme. As the wall-heat transfer q_f in this equation is ξ dependent, any ξ position in the spot can be used to determine τ_w. To eliminate the ξ dependence, the wall-heat transfer in equation (12) has been averaged between $x = x_0$ and the x-position downstream of the maximum hot-spot temperature, where the local temperature is equal to 50% of the maximum temperature. This uniquely fixes the wall-shear stress.

To determine the error due to the use of the similarity equation instead of the thermal boundary-layer equation, the wall-shear stress obtained with the similarity relation $c_{f,sim}$, has been compared to a reference value $c_{f,theor}$ given by the numerical solution of the velocity boundary-layer equation. It has been checked that the numerical solution for a Blasius flow reproduces the well-known wall-shear stress law

$$c_{f,theor} = 0.664\, Re_x^{-0.5} \tag{16}$$

with the wall-shear stress coefficient $c_f = \tau/\frac{1}{2}\rho_f U_e^{2-}$ and the local Reynolds number $Re_x = U_e x/\nu$.

Since equation (12) has been derived under the assumption of local heating, the influence of the hot-spot size on the wall-shear stress must be investigated. Figure 4 shows the resulting relative error $\Delta c_f = (c_{f,sim} - c_{f,theor})/c_{f,theor}$ in [%] as a function of w_{spot} for different free-stream velocities U_e ranging from 5–25 m s^{-1}. Here w_{spot} is defined as the distance between the two x-positions having a temperature of 50% of the maximum hot spot temperature T_{max}. The results show that the error Δc_f is below 1% for $w_{spot} \leqslant 1$ cm.

Next to the hot-spot size w_{spot} the maximum temperature in the hot-spot T_{max} and the time scale of the temperature decay t_{spot} are important parameters in this measurement technique. Here t_{spot} is defined as the time interval between turning off the laser and the decay of T_{max} to 50% of initial steady value. These parameters have to match both the assumption of local heating and the capabilities of the IR-camera; the application of the similarity theory imposes a small spot size w_{spot}, but because of the limited resolution of the IR-camera a large spot size is required as well. The reasons for the limited resolution are described in detail by Carlomagno and de Luca [8]. For the camera used in this investigation (AGEMA 880 LWB) the minimum angular size of the observed object is about 4 mrad, which corresponds to 1 mm in our experimental setup. Thus, the hot spot must be small enough to minimise the error due to using the similarity equation (12) (1 cm according to Fig. 4) but must also exceed the minimum object size (1 mm). In this investigation w_{spot} is 5–6 mm, which fits both limits.

Also for T_{max} a compromise has to be found. A high

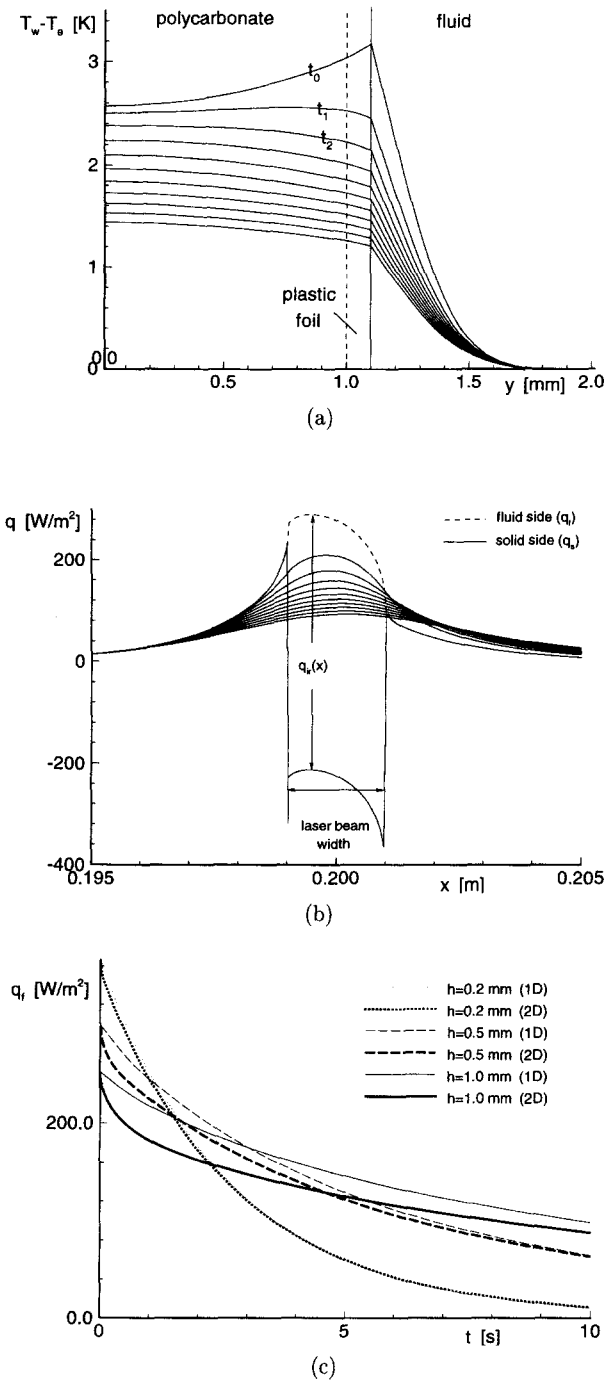

Fig. 3. Numerical simulation of the decay of a hot spot centred at $x = 0.2$ m for $U_e = 10$ m s^{-1}; (a) $T - T_e$ in y-direction in the solid and in the fluid (1 mm polycarbonate + 0.1 mm plastic foil), (b) corresponding q_f in x-direction in the fluid and in the solid, (c) comparison of q_f obtained with 1-D and 2-D heat-transfer equation for increasing thickness.

temperature is advantageous as it increases the signal-to-noise ratio of the IR-camera. We will see later that signal noise plays an important role in this measurement technique. But high temperatures also lead to changes in the density of the fluid, which is assumed to be constant in the boundary-layer equations and in the similarity equation. Furthermore a high temperature affects the behaviour of the flow, such as the transition location.

Not only the spatial resolution, but also the time response of the IR-camera is limited. The AGEMA 880 LWB needs 40 ms to measure one temperature

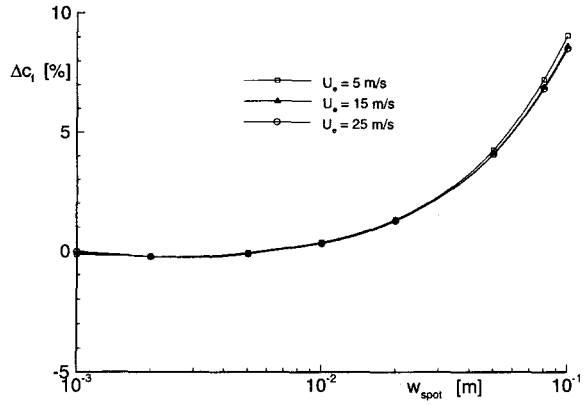

Fig. 4. Difference in the wall-shear stress coefficient at $x = 0.2$ m obtained with the boundary-layer equation and the similarity equation for different free-stream velocities.

distribution in the hot spot. Therefore the temperature decay of the hot spot can only be sampled by the camera if t_{spot} is large enough, say at least 1 s.

The parameters w_{spot}, T_{max} and t_{spot} are influenced by the flow conditions. They are even more influenced, however, by the properties of the solid like the density, the specific heat capacity, the thermal conductivity and the thickness. Table 1 presents the thermal properties of some solid materials tested in this study. These values were provided by the manufacturer of the materials. The properties of air are also given in the table.

To determine the required properties of the solid the full numerical simulation of the complete experiment has been performed. Since we originally used an 0.1 mm stainless steel plate with an 0.05 mm colour coating to increase the emissivity in a preliminary experiment, this combination of solids was simulated first. In that experiment we found large variations of w_{spot} for different x-positions on the plate, which turned out to be caused by tolerances of the thickness of the colour coating (being about 20%). This is clarified by the results of the numerical simulation presented in Fig. 5(a), which shows that w_{spot} is very sensitive to the thickness of the coating. Therefore the colour coating has been replaced by a 0.1 mm black dull plastic foil, which has nearly the same thermal properties as the colour coating, but which has a smaller thickness tolerance (<10%). Next to the coating, also the stainless steel has been replaced by polycarbonate to further reduce the sensitivity to the thickness tolerance of the coating. Since a certain minimum stiffness of the solid is required to set the measurement strip flush into the test plate the thickness of the polycarbonate was chosen as 1 mm, which is 10 times thicker than the stainless-steel solid. Figure 5(a) shows that now w_{spot} is nearly independent of the thickness of the coating. Another advantage of using polycarbonate instead of using stainless steel is shown in Fig. 5(b); t_{spot} is larger and also changes less with varying coating thickness.

Table 1. Thermal properties of air and some tested materials

	ρ [kg m^{-3}]	k [W m K^{-1}]	c [J kg K^{-1}]
Air	1.18	0.0262	1006
Stainless steel	7900	14	510
Polycarbonate	1200	0.20	1060
Colour coating	1400	0.16	1020

4.3. *Numerics required for the experimental method*

In the real experiment the temperature inside the fluid is not known. This means that the Neumann condition for the solid is not available. Since the IR-camera measures the surface temperature, this can be used as a Dirichlet boundary condition for the solid. Thus the temperature inside the solid can be calculated for each time step with the measured surface temperature and with an initial condition for the temperature inside the solid. To evaluate the initial condition for the solid the measured temperature distribution at steady-state conditions is prescribed. For an unsteady calculation of the solid, in which the steady boundary conditions are prescribed at each time step, the temperature inside the solid converges to a steady state for increasing time. Thus the final procedure to evaluate the wall-heat flux from the surface temperature measured by the IR-camera starts with the calculation of the initial temperature in the whole solid, using the measured steady-state temperature. Over the subsequent time new experimental Dirichlet boundary conditions are prescribed for each new time step and the temperature inside the solid is calculated.

To check this numerical procedure a numerical simulation was made in which Dirichlet boundary conditions are prescribed for the temperature in the solid, as will also occur in the data processing for a real IR-camera temperature measurement. In this case the temperature data of the camera are replaced by the temperature distribution at the surface of the object, as obtained in the described full numerical simulation. The heat flux in the solid as obtained with either Neumann or Dirichlet conditions was indeed the same.

In the experiment, the similarity equation (12), using an averaged q_f as described in Section 4.2, is applied to determine the wall-shear stress from the measured surface temperature and wall-heat transfer.

5. DATA PROCESSING

To derive the wall-shear stress from the measured surface temperature, a number of data processing steps has to be passed through. First the traversing system moves to the measurement point and the laser is switched on. Since the calculation of the heat transfer inside the solid, which is needed to determine q_f

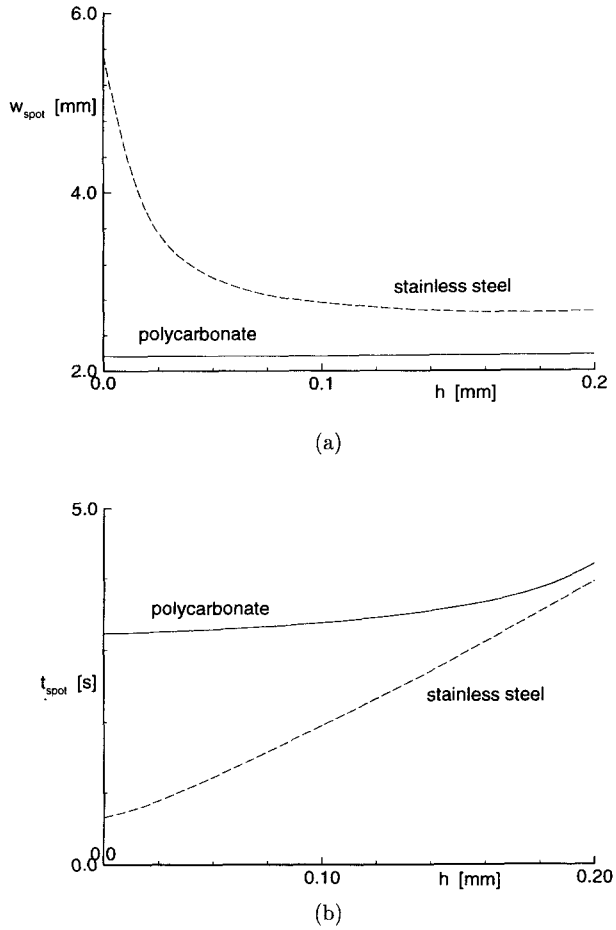

Fig. 5. Influence of the thickness h of the coating on (a) the width of the hot spot and (b) on the time scale of the temperature decay. Below the coating is either an 0.1 mm stainless steel or a 1 mm polycarbonate layer.

from the measured wall temperature, requires a steady state as initial condition for the Poisson equation, it is essential that the heating phase is sufficiently large (>3 min) for the steady state to have established. When steady-state is reached the temperature measurement is started and the data are stored. After a few distributions at steady-state conditions have been measured the laser is switched off.

To extract the required temperature boundary conditions for the calculation of the heat transfer to the fluid from the measured data the laser-turn-off-time (LTO) has to be determined. The IR-camera used in this investigation-scans the pixels of the field of view one after the other. This means that each pixel is generated at a different time. As long as the laser is switched on the temperature difference between one pixel and the same pixel in the previous picture is approximately zero. The first pixel, which has a larger temperature difference ΔT than the noise-equivalent-temperature-difference (NETD), serves as a criterion for the definition of the LTO. Thus the pixel which fulfils this criterion is scanned just after turning of the laser. Since it is known when each pixel is scanned the LTO can be determined.

With the given LTO the temperature boundary conditions can be determined. In the numerical evaluation of the unsteady heat transfer in the solid, the numerical time step was taken equal to the time interval between two temperature measurements of the camera (40 ms). This time step was checked to lead to an accurate numerical solution by repeating the computation with half the time step. Since the time between the LTO and the next temperature measurement of the camera is usually not equal to 40 ms, the Dirichlet conditions are evaluated at the numerical time levels by an interpolation between the measured data. Figure 6 presents the temperature decay in x-direction and the maximum temperature T_{max} in the hot-spot. The raw measured data are compared with the values for T_{max} after determining the LTO, after interpolation and after filtering the data.

As already mentioned, the present measurement technique is very sensitive to signal noise. This has two reasons. In the first place the scatter in the temperature